A Single Substrate Metasurface Dipole With Electrically Small Feeding Structure

Kok Loon Wong, *Member, IEEE*, Max J. Ammann, *Fellow, IEEE*, Ming Cao, and Fergal Lawlor, *Member, IEEE*

***Abstract*— Low-profile metasurface antennas are proposed for cellular base station applications. The dual-slant crossed-dipole antennas with four resonances employ both transverse magnetic (TM) and transverse electric (TE) surface wave modes. The metasurface dipole arms are capacitively coupled by an electrically small crossed-feed in a low-cost single substrate. The metasurface layer consists of $n \times n$ element arrays. The proposed low-profile (0.14λ) antennas can achieve a 10-dB impedance bandwidth of 57%, 58%, and 84% for metasurface dipole arms comprising 2 × 2, 3 × 3, and 4 × 4 elements, respectively. For cellular 65° sector base station applications where 14 dB is required, a bandwidth of 51%, 52%, and 63% for 2 × 2, 3 × 3, and 4 × 4 elements, respectively, is realized. For a single dipole with a reflector, the average boresight gain is 9 dBi, 3-dB beamwidth is 62° ± 7°, front-to-back ratio is better than 25 dB, and isolation is better than 35 dB over the frequency range of 1.7–2.7 GHz. For user equipment (UE) applications, extra low-profile (0.11λ) antennas are also presented.**

***Index Terms*— ±45°, 3-dB beamwidth, base station antenna, cross-polar discrimination (XPD), crossed dipole, dual polarized, dual slant, electrically small, front-to-back ratio, low profile, metasurface, resonance, surface wave, transverse electric (TE), transverse magnetic (TM), wideband antenna.**

I. Introduction

METASURFACE antennas have been widely investigated and developed due to low profile, wideband, and enhanced gain characteristics [1]. Moreover, dual-slant antennas are widely deployed in cellular base stations for polarization diversity [2] and due to identical patterns for both polarizations when compared to dual vertical and horizontal polarizations. Cellular base station antennas are required to have a return loss ≥14 dB across the full operating bandwidth [2], [3], i.e., 1.70–2.70 GHz (46%) for providing multiple services covering 4G and 5G to end users. This is due to power loss considerations and linear array gain stability across wide operating bandwidths [2]. The typical 3-dB beamwidth, front-to-back ratio (F/B), boresight cross-polar discrimination (XPD), and isolation recommendations for dual-slant 65° sector antenna are 65° ± 5°, ≥25, ≥20, and ≥26 dB, respectively [3]. A 3-dB beamwidth with minimum fluctuation is necessary for predictable network hand-off and mitigating adjacent cell interference to increase the system capacity [2]. F/B ratio is critical for frequency reuse characteristics and XPD is key for polarization diversity [2]. Good isolation reduces intermodulation products generated by the power amplifier stage [2]. Therefore, a high-performance dipole antenna is required to accommodate wide bandwidth applications with stable radiation patterns.

A dual-slant polarized metasurface antenna, employing two substrates with the dipole substrate separated from the suspended metasurface substrate, operates over 1.71–2.69 GHz [4] and 0.69–0.96 GHz [5]. Dual-polarized H–V antennas were reported with the metasurface layer above the dipole layer operating over 0.82–1.19 GHz [6] and a suspended metasurface layer below the dipole layer over 0.69–0.96 GHz [7]. Nasser and Chen [4], Zhu et al. [5], Liu et al. [6], and Chen and Yang [7] work on the principle whereby the half-wavelength crossed-dipole excites the metasurface to widen the impedance bandwidth. The reported isolation for [4], [5], [6], and [7] was >25 dB. The profile height and 10-dB impedance bandwidth were $0.11\lambda_0$ (46%) in [4], $0.09\lambda_0$ (41%) in [5], $0.05\lambda_0$ (37%) in [6], and $0.08\lambda_0$ (21%) in [7], respectively, where λ_0 is the lower edge frequency wavelength. However, it is difficult to achieve a 14-dB impedance bandwidth of 46% with these profile heights covering the range of 1.70–2.70 GHz. Moreover, Nasser and Chen [4], Zhu et al. [5], and Chen and Yang [7] excite two resonances, whereas Liu et al. [6] excite three resonances. The resonances are mainly in the surface wave mode, leaky wave mode, and dipole mode.

In [8], a metasurface based dipole was used, which excites three resonances to widen the impedance bandwidth. Particularly of interest, the transverse electric (TE) surface wave resonance within a finite high impedance surface (HIS) and a dipole resonance were generated to widen the impedance bandwidth of an HIS-based dipole antenna [9]. A suspended metasurface-based/HIS dipole antenna was proposed, where the impedance bandwidth was widened by combining the transverse magnetic (TM) and TE surface wave resonances within a metasurface layer [10]. In [8], [9], and [10], the

Manuscript received 8 September 2023; revised 20 May 2024; accepted 24 June 2024. Date of publication 10 July 2024; date of current version 9 August 2024. This work was supported by the Science Foundation Ireland under Grant 18/CRT/6222 and Grant 13/*RC*/2077_P2. *(Corresponding author: Kok Loon Wong.)*

Kok Loon Wong and Max J. Ammann are with the Antenna and High Frequency Research Centre, School of Electrical and Electronic Engineering, Technological University Dublin, Dublin 7, D07 EWV4 Ireland (e-mail: D21124367@mytudublin.ie; max.ammann@TUDublin.ie).

Ming Cao and Fergal Lawlor are with Alpha Wireless Ltd., Portlaoise, R32 DT0A Ireland (e-mail: cming@alphawireless.com; flawlor@alphawireless.com).

Color versions of one or more figures in this article are available at https://doi.org/10.1109/TAP.2024.3421904.

Digital Object Identifier 10.1109/TAP.2024.3421904

single-polarized dipoles and a half-wavelength dipole were used to excite the metasurface layer. The dipole and metasurface layers are commonly separated on different layers and substrates for [4], [5], [6], [7], [8], [9], and [10]. The profile height and 10-dB impedance bandwidth were $0.05\lambda_0$ (41%) in [8], $0.04\lambda_0$ (22%) in [9], and $0.06\lambda_0$ (34%) in [10], respectively. It is difficult to achieve a 14-dB impedance bandwidth of 46% due to the profile heights are low. In [11], the feed structure was used to generate a TM leaky wave resonance and a TE surface wave resonance was generated within the metasurface to achieve low profile with a wide impedance bandwidth. In [12], an antenna with low profile and wideband was achieved using multielement design.

In this article, a novel dual-slant metasurface radiator integrated on a single substrate is proposed, which excites four TE and TM surface wave resonances simultaneously to widen the impedance bandwidth. The antenna has a stable 3-dB beamwidth, good F/B, and isolation over the wide bandwidth >50%. Instead of using a half-wavelength dipole or crossed dipole to excite the metasurface layer, a novel electrically small $0.155\lambda_0$ crossed-feed structure comprising four chamfered patches is used. The radiator is fed by chamfered square patches and microstrip line baluns, which make a total antenna profile height of 0.14 λ_0 with a 14-dB impedance bandwidth better than 51% and cross-polar isolation better than 35 dB. The eigenmode solver was used to determine the surface wave resonances in the dispersion diagram. The square metasurface element is considered as a unit cell with periodicity and the dipole arm ($n \times n$) is considered as another unit cell. Lastly, a novel geometrical based equation is used to approximate the required metasurface element size to resonate at different frequencies on an electrically thin substrate. Different profile heights ($0.11\lambda_0$ and $0.14\lambda_0$) can be realized for wideband applications, and the performance is analyzed for various dipole sizes with different metasurface element arrays and profile heights. λ_0 is the wavelength at the lower edge frequency of 1.7 GHz.

II. Antenna Design

The geometry and dimensions of the antenna with 4 × 4 metasurface elements are shown in Fig. 1. The antenna consists of four metasurface dipole arms, four capacitive-coupled feeds, two integrated baluns, a base board, and a square reflector. In cellular applications, these would be arranged in a linear array covered by a radome and provide gains up to 18 dBi. Note that the *xoz*-plane and *yoz*-plane are defined as the azimuth plane (*AZ*-plane) and elevation plane (EL-plane), respectively.

Each dipole arm consists of 4 × 4 square patch elements with an interelement spacing of 0.3 mm, forming a metasurface, which is printed on the bottom layer of the FR4 substrate (0.5 mm thickness). The arms are fed using capacitively coupled chamfered square patches, which are printed on the top FR4 layer. Two diagonal metasurface dipole arms are used to form the −45° and +45° polarizations. In order to excite the radiator, baluns with an integrated Γ-shaped microstrip line are directly soldered to the chamfered square patches. The Γ-shaped line is formed by two sections of microstrip line connecting the base board to the shorted stub for impedance matching. A dual-polarized dipole is realized when one balun is connected to two diagonal chamfered top patches, which capacitively couple to the metasurface dipole arms to generate

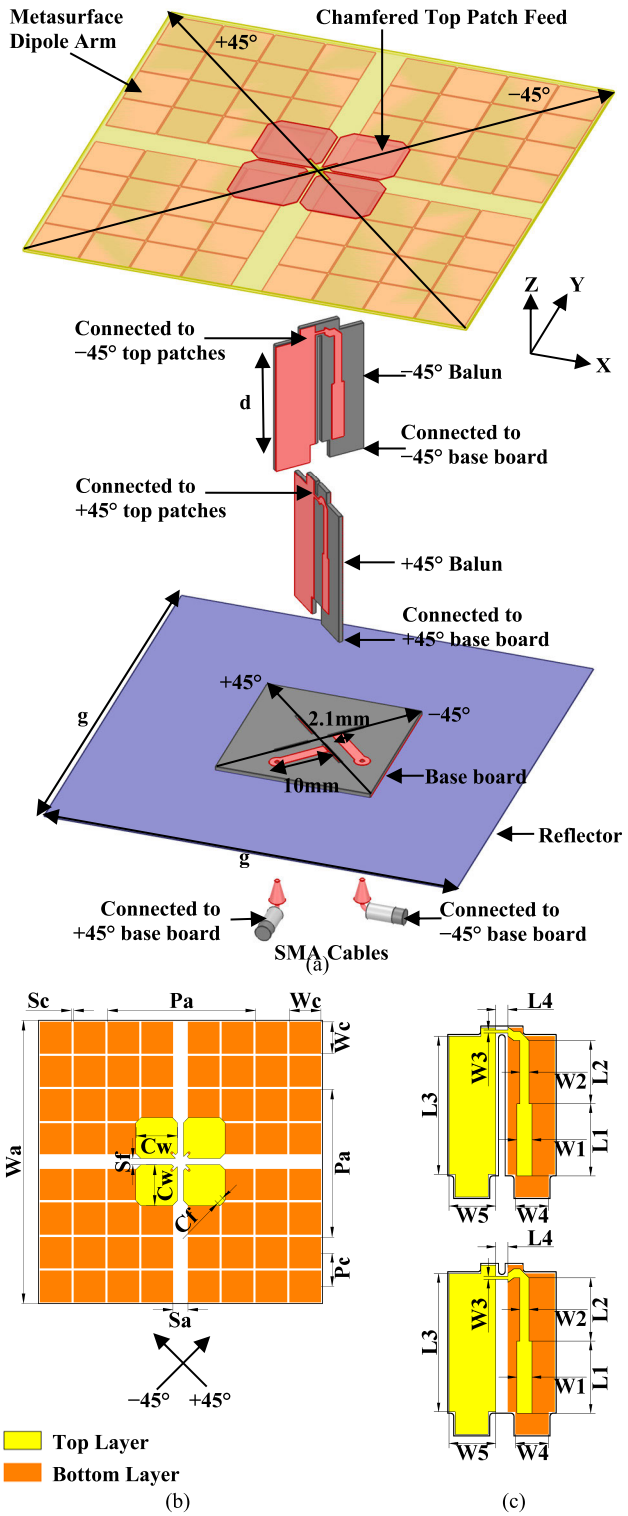

Fig. 1. Configuration of the antenna. (a) Three-dimensional exploded view. (b) Top view of crossed-dipole with metasurface dipole arms. d = 25, g =130, C_f = 2.8, C_w = 9.5, P_a = 45.3, P_c = 9.9, S_a = 6, S_c = 0.3, S_f = 0.6, W_a = 86, and W_c = 9.6 (unit: mm). (c) Side view of integrated baluns with microstrip feed. L_1 = 12, L_2 = 10.5, L_3 = 22.95, L_4 = 2, W_1 = 2.5, W_2 = 1.5, W_3 = 0.5, W_4 = 5.5, and W_5 = 7.75 (unit: mm).

−45° polarization and another balun connects to the other two diagonal arms to generate +45° polarization, as shown in Fig. 1(a). The ±45° baluns are connected to a ±45° microstrip line base board, as shown in Fig. 1(a). The microstrip baluns and base board are fabricated on PTFE substrates (Dk = 2.55 and 0.762 mm thickness). The base board with lower copper ground is mounted on an aluminum reflector. An SMA cable is connected to the base board for measurements.

III. Working Principle

A Brillouin zone dispersion diagram for the unit cells was obtained using the CST Eigenmode Solver. The S-parameters, electric field, and radiation patterns of metasurface antenna were modeled using the ANSYS HFSS software.

A. TM and TE Modes

The simulated E-fields for the 4 × 4 metasurface dipole are shown in Fig. 2, which is used to determine the metasurface TM and TE modes. Due to the antenna symmetry, only analyses of the −45° polarization excitation are shown. The simulated S_{11} resonant frequencies are 1.8, 2.4, 2.9, and 3.9 GHz.

Due to the E-fields being parallel to the −45° excited dipole for 1.8 and 2.4 GHz, Fig. 2(a), (b), and (i) shows that the dipole exhibits TM resonance and a broadside radiation pattern at 1.8 GHz, whereas Fig. 2(c), (d), and (j) shows a TM resonance and broadside pattern at 2.4 GHz. However, the orthogonal dipole E-field for the 2.9 GHz resonance is also parallel to the −45° axis, as shown in Fig. 2(e), (f), and (k), which indicates a TE resonance and broadside pattern.

The resonant mode at 3.9 GHz is shown in Fig. 2(g), (h), and (l). Based on E-field distribution in Fig. 2(g), the dipole exhibits TM resonance due to the fields being parallel to the −45° excited dipole with the orthogonal dipole arm fields in anti-phase. The radiation pattern is broadside in this mode, as shown in Fig. 2(l). However, the pattern is divided into four lobes with a simulated gain of 7.7 dBi and the maximum gain is not at boresight. Fig. 2(i)–(k) shows the broadside radiation pattern at 1.8, 2.4, and 2.9 GHz with a maximum boresight gain of 8.5, 8.7, and 9.1 dBi, respectively. The resonant mode at 3.9 GHz is unsuitable for base station antenna applications.

B. Surface Wave and Resonances

In this work, the dispersion characteristics of surface wave propagation on periodic structures comprising a metasurface dipole arm and a single element within a dipole arm are shown. A dipole arm with periodicity (Pa) comprising 2 × 2, 3 × 3, and 4 × 4 elements is considered as a unit cell shown in Fig. 3(a)–(c). The arm consists of elements with dimensions $W_c \times W_c$ and periodicity (P_c). They are placed at a distance d from the PEC ground plane of dimension $P_a \times P_a$. For a dipole arm consisting of 2 × 2, 3 × 3, and 4 × 4 elements, a unit cell comprising a single metasurface element of dimension $W_c \times W_c$ and periodicity (P_c) is placed at a distance d from the PEC ground plane of dimension $P_c \times P_c$, as shown in Fig. 3(g). All dimensions can be obtained from Fig. 1 and Table I. The dispersion diagrams for the 2 × 2, 3 × 3, and 4 × 4 element unit cell and the single element unit cell in the 2 × 2, 3 × 3, and 4 × 4 dipole arm over the Brillouin zone are illustrated in Fig. 3(a)–(f), respectively. The surface wave and leaky wave regions in the dispersion

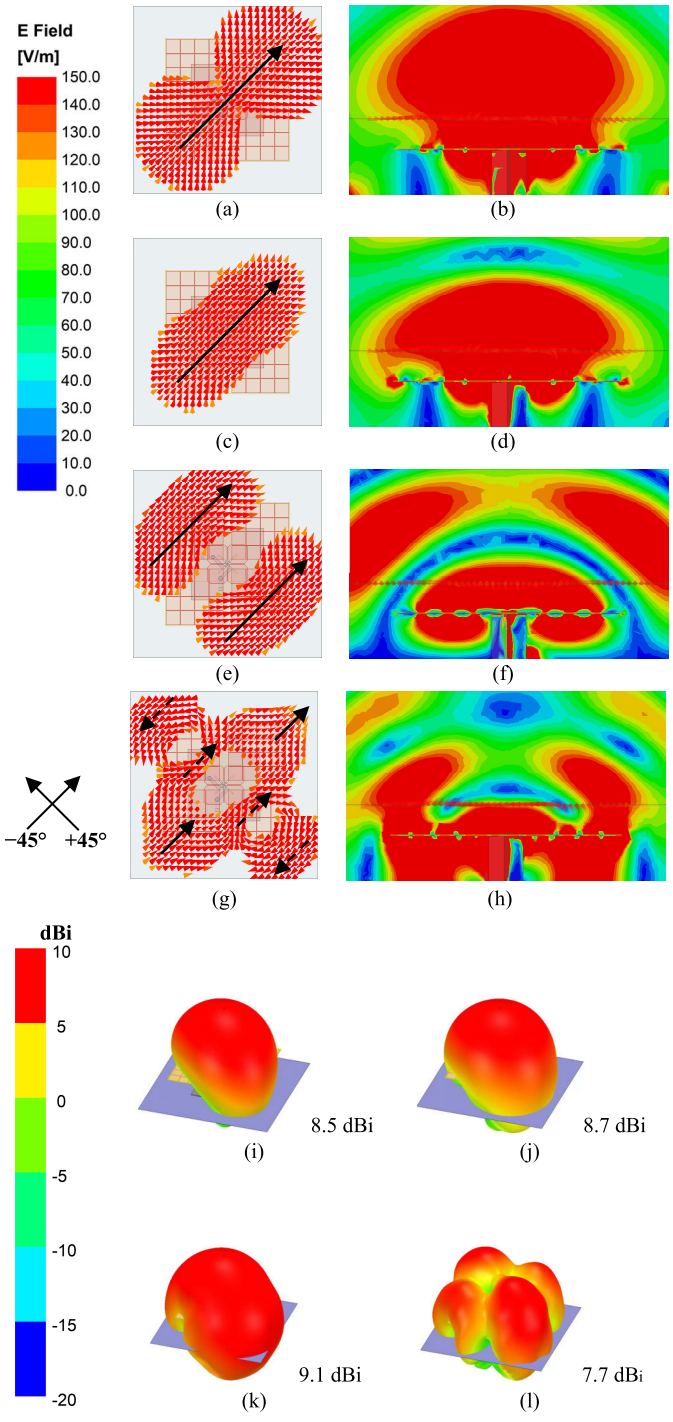

Fig. 2. E-field vector, E-field magnitude, and radiation pattern for −45° polarized dipole with dipole arm comprising 4 × 4 metasurface elements. Top view of dipole arm E-field vector at 40 mm above the ground plane (a) TM mode: 1.8 GHz. (c) TM mode: 2.4 GHz. (e) TE mode: 2.9 GHz. (g) TM mode: 3.9 GHz. Cross section view of dipole E-field magnitude in the direction of the excited dipole at (b) 1.8, (d) 2.4, and (h) 3.9 GHz and orthogonal direction to the excited dipole (f) at 2.9 GHz. Radiation patterns at (i) 1.8, (j) 2.4, (k) 2.9, and (l) 3.9 GHz.

TABLE I
(SEE FIG. 1 FOR PARAMETERS) DIMENSIONS FOR $n \times n$ METASURFACE ELEMENTS ($d = 0.14\lambda_0$)

n	Dimensions (mm)					
	C_w	C_f	S_c	S_f	W_a	W_c
2	7.6	0.3	0.3	0.4	74	16.6
3	11.8	0.1	0.3	1.5	84	12.5
4	9.5	2.8	0.3	0.6	86	9.6
5	9.5	2.8	0.3	0.8	90	8.1
6	11	2.8	0.3	1.5	94	7.0

diagram can be determined by [13]

$$k_0^2 = \omega^2\varepsilon_0\mu_0 < k_x^2 + k_y^2 \quad \text{(Surface wave)} \tag{1}$$
$$k_0^2 = \omega^2\varepsilon_0\mu_0 > k_x^2 + k_y^2 \quad \text{(Leaky wave)} \tag{2}$$
$$k_0^2 = \omega^2\varepsilon_0\mu_0 = k_x^2 + k_y^2 \quad \text{(Light line)} \tag{3}$$
$$k_0 = \omega\sqrt{\varepsilon_0\mu_0} = 2\pi f\sqrt{\varepsilon_0\mu_0} \tag{4}$$

where k_0 is the free space wavenumber. k_x and k_y are the wavenumbers along the x- and y-axes, respectively, as shown in Fig. 1(a). f is the frequency of the electromagnetic wave in Hz, ε_0 and μ_0 are the permittivity and permeability of free space, respectively. The surface wave and leaky wave regions are separated by the light line in the dispersion diagram [13].

The three specific points (Γ, X, and M) in Fig. 3(a)–(c) can be determined by [13]

$$\Gamma: k_x = 0, \quad k_y = 0 \tag{5}$$
$$\text{X}: k_x = \frac{2\pi}{(W+g)}, \quad k_y = 0 \tag{6}$$
$$\text{M}: k_x = \frac{2\pi}{(W+g)}, \quad k_y = \frac{2\pi}{(W+g)} \tag{7}$$

where $(W + g)$ is the periodicity of a unit cell. It is replaced by P_a and P_c in this article.

First, the dispersion diagram in Fig. 3(a)–(c) is investigated. It is understood that 2 × 2 unit cells (dipole arms) with periodicity, P_a are required to form a $\lambda/2$ metasurface dipole, as illustrated in Fig. 1. When the −45° polarized dipole is excited, the +45° polarized dipole acts as a parasitic dipole. The resonances are determined by the size of ±45° planar dipoles. Therefore, the three specific points, where resonances (f_1–f_3) occur, can be referred to the dispersion diagram shown in Fig. 3(a)–(c), respectively

$$\text{f}_1: k_x = \frac{\pi}{P_a}, \quad k_y = 0 \quad (1/2 \text{ of } \Gamma \text{ to X}) \tag{8}$$
$$\text{f}_2, \text{f}_3: k_x = \frac{\pi}{P_a}, \quad k_y = \frac{\pi}{P_a} \quad (1/2 \text{ of M to } \Gamma). \tag{9}$$

The resonant frequencies f_1–f_3 (2 × 2, 3 × 3, and 4 × 4 dipole elements) obtained from dispersion diagram, measured, and simulated S_{11} and S_{22} are summarized in Tables II–IV. Since $k_x^2 + k_y^2 > k_0^2$ for f_1–f_3 (all cases), all resonant frequencies are surface wave resonance, which satisfy the condition outlined in (1).

Second, the dispersion diagram of a single element unit cell is investigated. There are 2 × 2, 3 × 3, and 4 × 4 metasurface elements with two, three, and four periodicities, P_c integrated within a dipole arm, as illustrated in Fig. 3(a)–(c), respectively.

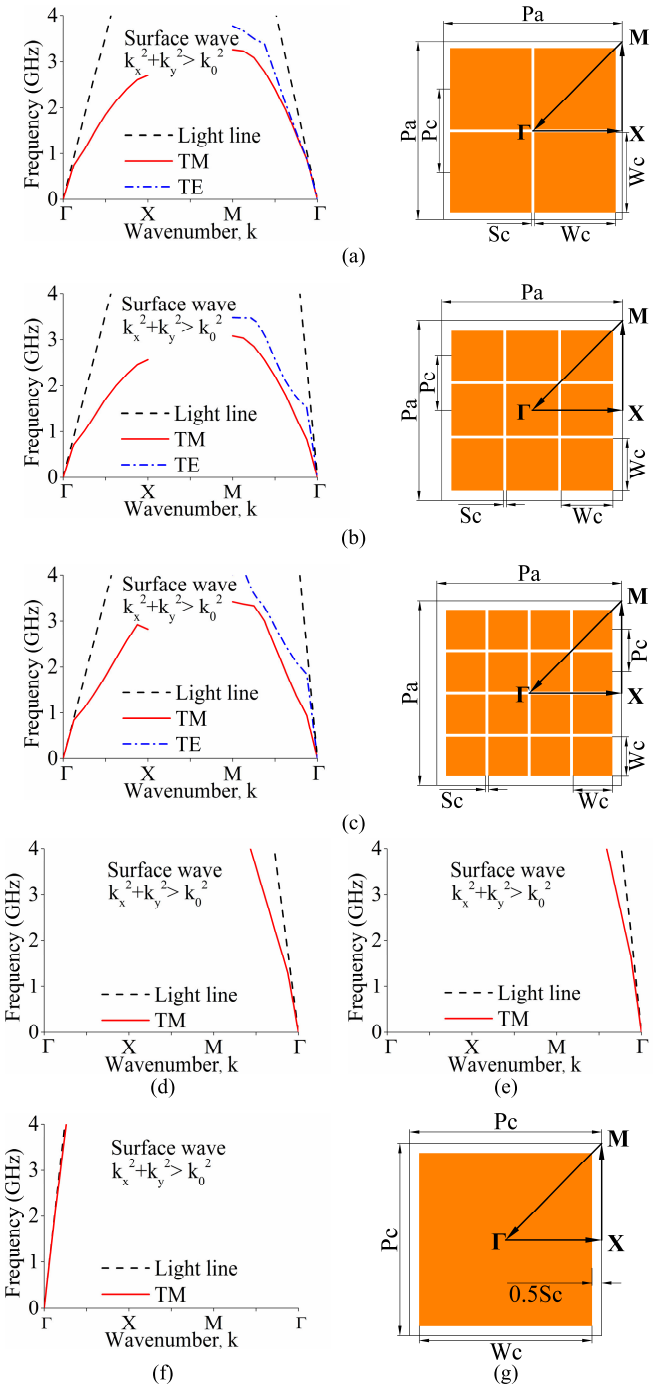

Fig. 3. Dispersion diagram of a dipole with (a) 2 × 2 element unit cell with associated geometry, (b) 3 × 3 element unit cell with associated geometry, and (c) 4 × 4 element unit cell with associated geometry. Dispersion diagram of a single element unit cell in a dipole with (d) 2 × 2 elements, (e) 3 × 3 elements, and (f) 4 × 4 elements. The associated geometry for (d)–(f) is shown in (g).

Therefore, the specific point, where resonance, f_4 occurs, can be referred to a dispersion diagram shown in Fig. 3(d)–(f), respectively

$$\text{f}_{4(2\times2\,elements)}: \; k_x = \frac{\pi}{P_c}, \quad k_y = \frac{\pi}{P_c} \quad (1/2 \text{ of M to } \Gamma) \tag{10}$$
$$\text{f}_{4(3\times3\,elements)}: \; k_x = \frac{2\pi}{3P_c}, \quad k_y = \frac{2\pi}{3P_c} \quad (2/3 \text{ of M to } \Gamma) \tag{11}$$

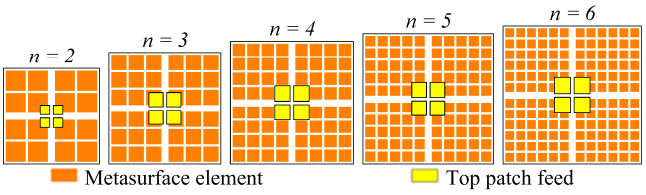

Fig. 4. Antenna geometry showing dipole arms with $n \times n$ elements.

TABLE II
RESONANCES FOR THE 2 × 2 ELEMENT DIPOLE

	Dispersion Diagram	Meas. $\|S_{11}\|$	Meas. $\|S_{22}\|$	Sim. $\|S_{11}\|$	Sim. $\|S_{22}\|$
f_1 (GHz)	1.9	1.8	1.8	1.8	1.8
f_2 (GHz)	2.4	2.3	2.3	2.3	2.3
f_3 (GHz)	2.7	2.7	2.7	2.7	2.6
f_4 (GHz)	3.6	3.8	3.8	3.7	3.7

TABLE III
RESONANCES FOR THE 3 × 3 ELEMENT DIPOLE

	Dispersion Diagram	Meas. $\|S_{11}\|$	Meas. $\|S_{22}\|$	Sim. $\|S_{11}\|$	Sim. $\|S_{22}\|$
f_1 (GHz)	1.7	1.7	1.7	1.8	1.8
f_2 (GHz)	2.2	2.3	2.3	2.3	2.3
f_3 (GHz)	2.6	2.6	2.6	2.6	2.7
f_4 (GHz)	3.4	3.5	3.6	3.5	3.5

TABLE IV
RESONANCES FOR THE 4 × 4 ELEMENT DIPOLE

	Dispersion Diagram	Meas. $\|S_{11}\|$	Meas. $\|S_{22}\|$	Sim. $\|S_{11}\|$	Sim. $\|S_{22}\|$
f_1 (GHz)	1.8	1.8	1.8	1.8	1.8
f_2 (GHz)	2.4	2.4	2.4	2.4	2.4
f_3 (GHz)	2.9	2.9	3.0	2.9	3.0
f_4 (GHz)	3.9	3.9	4.0	3.9	4.0

$$\mathrm{f}_{4(4\times4\,elements)}:\ k_x = \frac{\pi}{2P_c}, \quad k_y = 0 \quad (1/4 \text{ of } \Gamma \text{ to X}). \tag{12}$$

The resonant frequency f_4 (metasurface dipole integrated with 2 × 2, 3 × 3, and 4 × 4 elements) is obtained from dispersion diagram, and the measured and simulated S_{11} and S_{22} are summarized in Tables II–IV. Since $k_x^2 + k_y^2 > k_0^2$ for f_4 (all cases), the resonance is surface wave.

Overall, it can be concluded that all metasurface dipoles excite resonances at f_1, f_2, and f_4, which are TM surface wave resonances, whereas f_3 is a TE surface wave resonance.

IV. PARAMETER STUDY

A. Metasurface Element Width, W_c

It is possible to design different metasurface dipole arm sizes with the same profile height (d), achieving a 14-dB impedance bandwidth consistently using different ranges of metasurface element separations (S_c), metasurface element width (W_c), dipole arm separation (S_a), and dipole width (W_a).

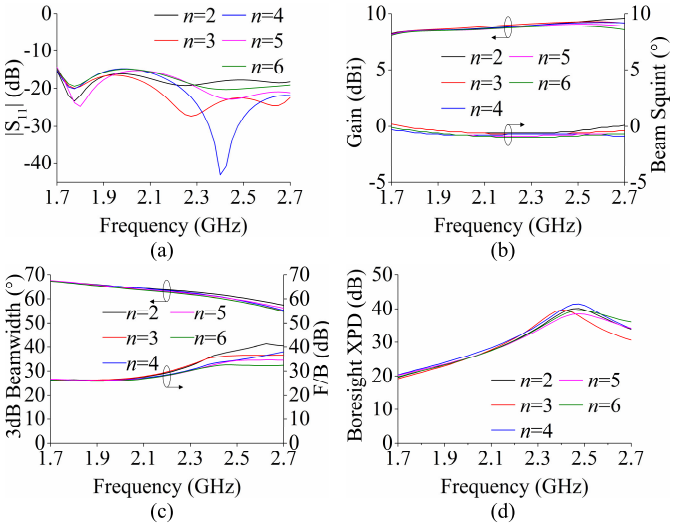

Fig. 5. (a) S_{11} ($d = 0.14\lambda_0$). (b) Gain and beam squint ($d = 0.14\lambda_0$). (c) 3-dB beamwidth and F/B ratio ($d = 0.14\lambda_0$). (d) Boresight XPD ($d = 0.14\lambda_0$).

A geometrical-based equation is derived to approximate the required metasurface element size to resonate at different frequencies on an electrically thin substrate

$$W_c = \frac{\left(\frac{C_0}{f_L \times N} - S_a\right)}{n} - S_c, \quad \mathrm{S_c} \le 1 \text{ mm}, \text{ and } \mathrm{W_a} \le \lambda_0/2 \tag{13}$$

where c_0 is the speed of light, f_L is the lower edge resonant frequency, $N = 4$ is the total number of dipole arms, and $n \ge 2$ is the number of $n \times n$ metasurface element arrays in a dipole arm.

Various metasurface dipole arm sizes with the same profile height of $0.14\lambda_0$ ($d = 25$ mm) and metasurface element separations ($S_c = 0.3$ mm) on a $0.73\lambda_0 \times 0.73\lambda_0$ ground plane were investigated. By using (13), the optimized geometry and dimensional parameters of the metasurface dipole arm are shown in Figs. 1 and 4 and Table I with other parameters remaining unchanged.

The performances for various dipole arms with $n \times n$ elements were analyzed. The simulated 14-dB impedance bandwidths for various types of $n = 2$, 3, 4, 5, and 6 are 50% (1.69–2.83 GHz), 51% (1.69–2.84 GHz), 61% (1.7–3.18 GHz), 59% (1.70–3.11 GHz), and 67% (1.69–3.39 GHz), respectively. The impedance bandwidth is better than 14 dB within the band of interest (BOI) 1.7–2.7 GHz for each configuration, as shown in Fig. 5(a).

The simulated radiation properties are illustrated in Fig. 5(b)–(d). Within the BOI, the simulated average gains for $n = 2$, 3, 4, 5, and 6 are 8.9, 8.9, 8.8, 8.7, and 8.6 dBi, respectively, as shown in Fig. 5(b). The 3-dB beamwidth is 55°–68° for all configuration types and it is similar over the BOI range, as shown in Fig. 5(c). The gain decreases slightly as the antenna size increases from $n = 4$ to 6 due to the wider 10-dB beamwidth at the higher end (the average 10-dB beamwidths from 2.5 to 2.7 GHz for $n = 2$, 3, 4, 5, and 6 are 115°, 115°, 115°, 120°, and 122°, respectively). The beam

TABLE V

RADIATION PROPERTIES FOR $n \times n$ METASURFACE ELEMENTS ($d = 0.14\lambda_0$)

	n=2	*n=3*	*n=4*
Gain (dBi)	8.9±0.7	8.7±0.56	8.7±0.54
14 dB Bandwidth (%)	50	51	61
3 dB Beamwidth (°)	63±5	61±6	61±6
Boresight XPD (dB)	30±10	29±10	31±10
F/B (dB)	34±7	31±5	32±6

TABLE VI

(SEE FIG. 1 FOR PARAMETERS) DIMENSIONS FOR $n \times n$ METASURFACE ELEMENTS ($d = 0.11\lambda_0$)

n	Dimensions (mm)		
	L_1	L_3	W_1
2	7.0	17.95	1.5
3	7.0	17.95	1.5
4	7.0	17.95	2.5

squint, the F/B ratio at ±30° from the back, and the boresight XPD across the BOI for $n = 2$–6 are shown in Fig. 5(b)–(d). These are well within the specification.

The next step is antenna selection and comparison. Since the antenna is mainly designed for cellular base station antenna application and in order to avoid grating lobes at the upper band edges for higher electrical tilt, it is better to have the dipole size, $W_a \leq \lambda_0/2$. So, $n = 2$, 3, and 4 are considered after eliminating $n = 5$ and 6 ($W_a > \lambda_0/2$).

Further in-depth analyses were carried out for $n = 2$–4. The simulated impedance bandwidth and electrical properties are summarized in Table V for comparison. It can be observed that the $n = 2$ configuration has better gain compared to the others. Dipole with $n = 3$ and 4 configurations has similar gain. Based on the 3-dB beamwidth recommendation [3], the simulated beamwidth for $n = 2$–4 is close to the recommendation. The simulated F/B and boresight XPD for all antenna configurations are >26 and >20 dB (>19 dB for $n = 3$), respectively. However, all recommendations in [3] are based on an antenna with 14-dB impedance bandwidth of 24%. Thus, the properties shown in Table V are acceptable for an antenna with 14-dB impedance bandwidth of more than 50%. Based on the above analyses, antenna gain and impedance bandwidth are the key factors in antenna selection. Besides that, antenna size is also important. The metasurface elements with 2 × 2 (smallest dipole size), 3 × 3, and 4 × 4 (widest 14-dB bandwidth) were chosen for fabrication to verify the results between simulation and measurement.

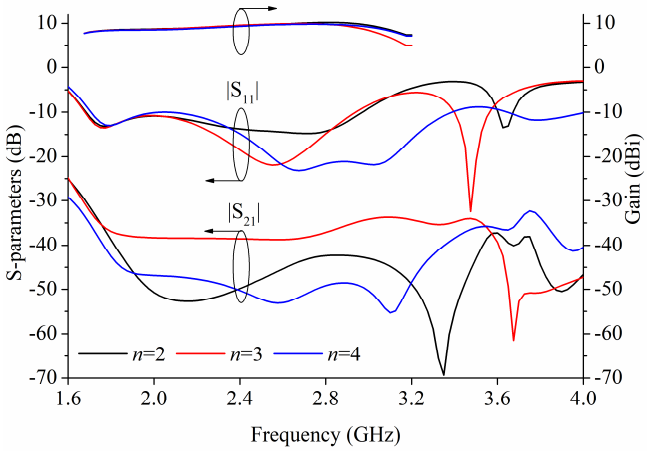

Fig. 6. Gain and S-parameters ($d = 0.11\lambda_0$).

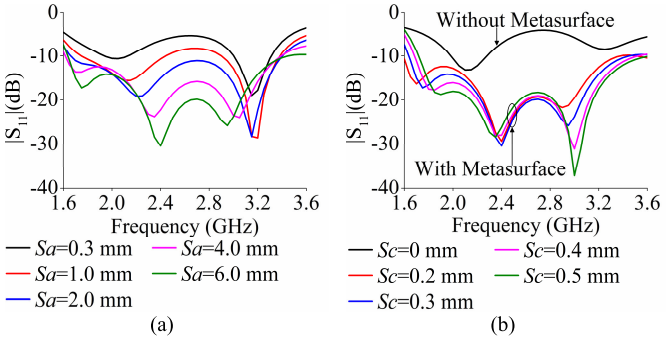

Fig. 7. S_{11} for a 4 × 4 metasurface dipole with different (a) S_a and (b) S_c values.

B. Reducing Profile Height, d

The profile height can be further reduced to 20 mm ($0.11\lambda_0$) by adjusting and impedance matching (L_1, L_3, and W_1) for the same dipole size (Table I). As shown in Fig. 6, a wide impedance characteristic (10 dB) and reasonable average gain >8.9 dBi for $n = 2$–4 can be obtained for less stringent applications like antennas for user equipment (UE) applications, which usually require extra low-profile antennas in the limited space and wideband operation to cover different services. The $0.11\lambda_0$ profile antenna dimensions for different $n \times n$ configurations are shown in Table VI, and the simulated electrical properties for each case within the BOI are summarized in Table VII.

The 3-dB beamwidth is 54°–68° for all configuration types and it is similar over the BOI. The beam squint is within ±2° and the boresight XPD > 17 dB for all configurations.

C. Varying Dipole Arm Separation S_a, and Element Separation, S_c

The parameters from Fig. 1 are used for S_{11} simulations, whereas the other parameters remain unchanged. The simulated S_{11} for a 4 × 4 metasurface dipole with different S_a and S_c values is shown in Fig. 7(a) and (b), respectively.

For a parameter sweep of S_a, the 10-dB bandwidth for $S_a = 0.3$, 1, 2, 4, and 6 mm is 19%, 48%, 69%, 71%, and 71%, respectively, whereas the 14-dB bandwidth is 54%, 21%, 32%, 45%, and 62%, respectively. When $S_a = 0.3$ mm, it can be considered as a center-fed metasurface patch antenna. When $S_a \geq 1$ mm, the configurations are considered as a dipole antenna. The impedance bandwidth is getting better with increased S_a due to reduced coupling between ±45° polarized dipoles. $S_a = 6$ mm was chosen in

TABLE VII
COMPARISON WITH STATE OF THE ART

Ref.	10 dB Impedance bandwidth (%)	14 dB Impedance bandwidth (%)	Polarization	Average gain (dBi)	Isolation (dB)	Size (λ_0^2)	Profile height (λ_0)	Ground plane size (λ_0^2)	3 dB beamwidth (°)	Boresight XPD (dB)	F/B @ ±30° (dB)	Resonances (Substrate) Feed length
0.14 λ_0 Ant. I (2×2 elements)	57 (1.64–2.94 GHz) (meas.)	51 (1.69–2.84 GHz) (meas.)	DS	9.1 (meas.)	>35 (meas.) (14 dB bandwidth)	0.42^2	0.14	0.73^2	63±7 (meas.)	>20 (meas.)	>25 (meas.)	4 (Single) 0.092 λ_0
0.14 λ_0 Ant. II (3×3 elements)	58 (1.62–2.95 GHz) (meas.)	52 (1.67–2.83 GHz) (meas.)	DS	9.1 (meas.)	>34 (meas.) (14 dB bandwidth)	0.47^2	0.14	0.73^2	61±8 (meas.)	>20 (meas.)	>25 (meas.)	4 (Single) 0.14 λ_0
0.14 λ_0 Ant. III (4×4 elements)	84 (1.63–4.0 GHz) (meas.)	63 (1.69–3.23 GHz) (meas.)	DS	9 (meas.)	>35 (meas.) (14 dB bandwidth)	0.48^2	0.14	0.73^2	62±7 (meas.)	>20 (meas.)	>25 (meas.)	4 (Single) 0.155 λ_0
0.11 λ_0 Ant. IV (2×2 elements)	54 (1.7–2.96 GHz) (sim.)	14.0 (2.45–2.82 GHz) (sim.)	DS	9 (sim.)	>31 (sim.) (10 dB bandwidth)	0.42^2	0.11	0.73^2	62±6 (sim.)	>17 (sim.)	>26 (sim.)	3 (Single) 0.092 λ_0
0.11 λ_0 Ant. V (3×3 elements)	55 (1.68–2.94 GHz) (sim.)	23 (2.25–2.82 GHz) (sim.)	DS	9 (sim.)	>31 (sim.) (10 dB bandwidth)	0.47^2	0.11	0.73^2	61±7 (sim.)	>17 (sim.)	>26 (sim.)	3 (Single) 0.14 λ_0
0.11 λ_0 Ant. VI (4×4 elements)	66 (1.71–3.39 GHz) (sim.)	31 (2.37–3.25 GHz) (sim.)	DS	8.9 (sim.)	>35 (sim.) (10 dB bandwidth)	0.48^2	0.11	0.73^2	61±7 (sim.)	>18 (sim.)	>26 (sim.)	4 (Single) 0.155 λ_0
[4]	46 (1.71–2.69 GHz)	20 (2.30–2.80 GHz)	DS	9	>27 (10 dB bandwidth)	0.51^2	0.11	0.86^2	56±12	>18	>17	2 (Dual) X-Dipole
[5]	41 (0.66–1 GHz)	22	DS	8.3	>25 (10 dB bandwidth)	0.4^2	0.09	0.74^2	64.5±3.5	>28	>12	2 (Dual) X-Dipole
[6]	37 (0.82–1.19 GHz)	12 (0.82–0.92 GHz)	DP	9.3	>26.7 (10 dB bandwidth)	0.49^2	0.05	0.53^2	55±12	>25	>19	3 (Single) X-Dipole
[7]	21 (4.31–5.32 GHz)	8 (4.4–4.6 GHz)	DP	6	>40 (10 dB bandwidth)	0.56^2	0.08	0.56^2	100	>20	>23	2 (Dual) X-Dipole
[8]	41 (4.48–6.8 GHz)	3 (4.55–4.7 GHz)	SP	10.1	N/A	1.4 × 1.22	0.05	1.4 × 1.22	45–60	>17	>30	3 (Single) ½ λ Dipole
[9]	22 (1.28–1.6 GHz)	2 (1.34–1.36 GHz)	SP	8	N/A	0.21 × 0.01	0.04	0.63^2	N/A	N/A	N/A	2 (Dual) ½ λ Dipole
[10]	34 (4.15–5.85 GHz)	17 (4.2–5 GHz)	SP	8.5	N/A	1.04 × 0.49	0.06	1.11^2	55–80	>20	>18	2 (Dual) ½ λ Dipole
[11]	21 (4.9–6.1 GHz)	18 (5.05–6.05 GHz)	SP	7.8	N/A	1.09^2	0.04	1.09^2	60–80	>13	>18	2 (Single) 0.16 λ_0

DS: Dual-slant, DP: Dual-polarized, SP: Single-polarized

this work due to the 14-dB requirement in base station antenna applications.

By sweeping the S_c parameter, the 10-dB bandwidth for $S_c = 0$, 0.2, 0.3, 0.4, and 0.5 mm is 14%, 72%, 71%, 71%, and 71%, respectively, whereas the 14-dB bandwidth is 0%, 50%, 62%, 61%, and 60%, respectively. The 10-dB bandwidth (>70%) is almost similar for $S_c \geq 0.2$ mm. The 14-dB bandwidth is >49% for $S_c \geq 0.2$ mm. Therefore, $S_c \geq 0.2$ mm is required in the $n \times n$ metasurface dipole for a good impedance bandwidth. When $S_c = 0$, this configuration is considered as a low-profile conventional dipole without a metasurface layer. The impedance bandwidth is worse due to the profile height and dipole size is not ideal for 1.7–2.7 GHz.

D. Varying Top Patch Feed Width, C_w

The parameters from Fig. 1 are used for S_{11} simulation, whereas other parameters remain unchanged. The simulated S_{11} for a 4 × 4 dipole with different C_w is shown in Fig. 8.

A parameter sweep of the top patch feed width, C_w was made. As explained in Section III-B, there are four surface wave resonances (1.8, 2.4, 2.9, and 3.9 GHz) generated by the metasurface layer without the top patch feed. The two diagonal chamfered top patches excite the metasurface layer to generate either −45° or +45° polarization. The top patch feed width, C_w is optimized to get similar resonances, which are obtained in Fig. 3(c) and (f). Fig. 8 shows that when the top patch is

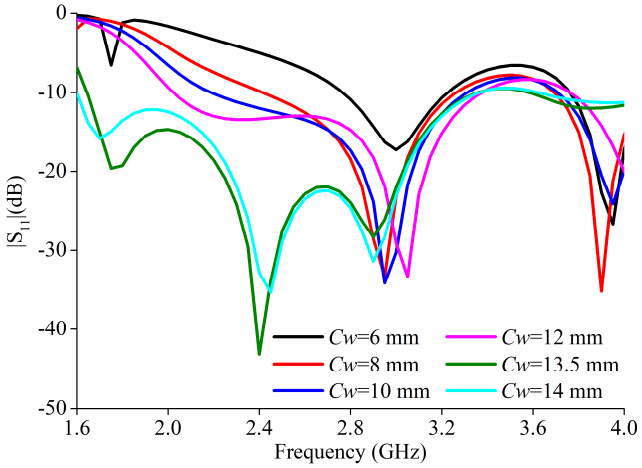

Fig. 8. S_{11} for a 4 × 4 metasurface dipole with different C_w values.

Fig. 9. Top and side view of dipole prototypes with 2 × 2, 3 × 3, and 4 × 4 elements (from left to right).

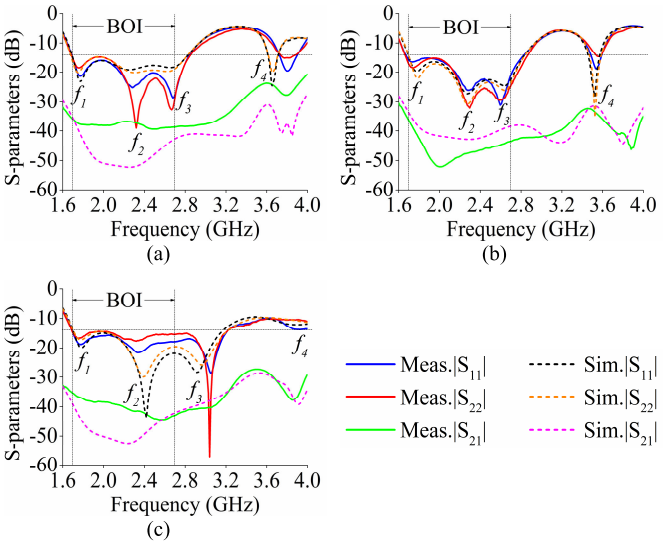

Fig. 10. Measured and simulated S-parameters for dipole with (a) 2 × 2 elements, (b) 3 × 3 elements, and (c) 4 × 4 elements.

small (C_w = 2, 4, and 6 mm) and the crossed-feed structure comprising four patches is electrically smaller than $0.12\lambda_0$, the metasurface layer generates two resonant modes at high frequencies 2.9 and 3.9 GHz. The metasurface layer starts to generate a third resonant mode at 2.4 GHz when $C_w = 8$ mm and the crossed feed electrical length is $0.14\lambda_0$. The fourth mode at 1.8 GHz is generated when $C_w = 9.5$ mm. There is an impedance mismatch when $C_w = 10$ mm and the crossed-feed electrical length is $0.16\lambda_0$. As a result, the capacitive coupling from the square top patch feed layer to the metasurface layer is mainly for impedance matching and excites the metasurface layer. C_w = 9.5 mm was chosen in this work due to the better matching in BOI, and the resonant frequencies from the dispersion diagrams and S_{11} are in good agreement. It is equivalent to a total electrical length of $0.155\lambda_0$ for a crossed-feed structure.

It can be concluded that the resonances and matching are dependent on C_w. The $0.155\lambda_0$ crossed-feed patches excite the metasurface layer and the metasurface layer generates all resonances.

V. Results and Discussion

A. Dipole Arms Comprising 2 × 2 Metasurface Elements

Fig. 9 shows the fabricated antennas with 25-mm profile, whereas Fig. 10(a) shows the measured and simulated S-parameters. The overall measured and simulated 10-dB bandwidth for −45° polarization is 57% (1.64–2.94 GHz) and 56% (1.65–2.94 GHz), respectively, and for +45° is 58% (1.64–2.98 GHz) and 57% (1.64–2.94 GHz), respectively. The measured and simulated isolation is better than 34 and 32 dB, respectively. Since the antenna is designed for base station applications, the measured and simulated 14-dB bandwidth for −45° polarization is 51% (1.69–2.84 GHz) and 50% (1.69–2.83 GHz), respectively, and for +45° is 52% (1.68–2.86 GHz) and 51% (1.68–2.83 GHz), respectively. The measured and simulated isolation is better than 35 dB.

The gain curves for ±45° polarizations are shown in Fig. 11(a). Due to the antenna symmetry, only radiation patterns of the −45° polarization are shown in Fig. 12(a). For patterns within the BOI for both *AZ*- and EL-planes, the measured gain is 8.9 ± 0.8 dBi, the 3-dB beamwidth is 63° ± 7°, the beam squint is within ±2°, the boresight XPD is greater 20 dB, and the F/B at ±30° range from the back is greater than 25 dB.

B. Dipole Arms Comprising 3 × 3 Metasurface Elements

Fig. 10(b) shows the measured and simulated S-parameters for the 3 × 3 metasurface dipole. The overall measured and simulated 10-dB bandwidth for −45° polarization is 58% (1.62–2.95 GHz) and 56% (1.65–2.94 GHz), respectively, and for +45° is 58% (1.62–2.95 GHz) and 56% (1.65–2.94 GHz), respectively. The measured and simulated isolation is better than 32 and 31 dB, respectively. The measured and simulated 14-dB bandwidth for −45° polarization is 52% (1.67–2.83 GHz) and 51% (1.69–2.84 GHz), respectively, and for +45° is 53% (1.66–2.87 GHz) and 50% (1.70–2.84 GHz), respectively. The measured and simulated isolation is better than 34 and 33 dB, respectively.

The gain curves for ±45° polarizations are shown in Fig. 11(b). The patterns within the BOI for both *AZ*- and EL-planes are shown in Fig. 12(b), the measured gain is 8.9 ± 0.6 dBi, the 3-dB beamwidth is 61° ± 8°, the beam squint is within ±2°, the boresight XPD is greater

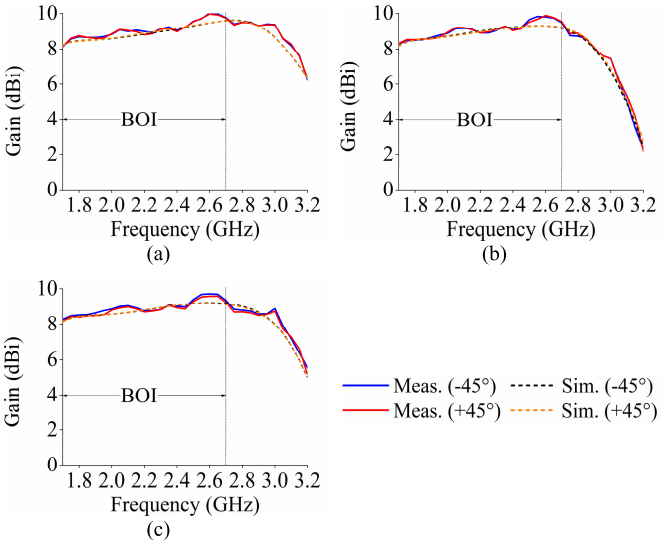

Fig. 11. Measured and simulated gain for dipole with (a) 2 × 2 elements, (b) 3 × 3 elements, and (c) 4 × 4 elements.

20 dB, and the F/B at ±30° range from the back is greater than 25 dB.

C. Dipole Arms Comprising 4 × 4 Metasurface Elements

Fig. 10(c) shows the measured and simulated S-parameters for the 4 × 4 metasurface dipole. The overall measured and simulated 10-dB impedance bandwidth for −45° polarization is 84% (1.64–4.0 GHz) and 69% (1.65–3.38 GHz), respectively, and for +45° polarization is 84% (1.63–4.0 GHz) and 72% (1.65–3.49 GHz), respectively. The measured and simulated isolation is better than 27 and 30 dB, respectively. The measured and simulated 14-dB bandwidth for −45° polarization is 63% (1.69–3.23 GHz) and 61% (1.7–3.18 GHz), respectively, and for +45° is 63% (1.69–3.23 GHz) and 62% (1.7–3.23 GHz), respectively. The measured and simulated isolation is better than 35 dB.

The gain curves for ±45° polarizations are shown in Fig. 11(c). For radiation patterns within the BOI for both *AZ*- and EL-planes, as shown in Fig. 12(c), the measured gain is 8.8 ± 0.55 dBi, the 3-dB beamwidth is 62° ± 7°, the beam squint is within ±2°, the boresight XPD is greater 20 dB, and the F/B at ±30° range from the back is greater than 25 dB.

It can be observed that the upper measured resonance, f_3 is 3 GHz for dipole with 4 × 4 elements, compared to 2.7 and 2.6 GHz for dipoles with 2 × 2 and 3 × 3 elements, respectively. As a result, a much wider impedance bandwidth is achieved compared to dipoles with 2 × 2 and 3 × 3 elements.

D. Comparison With State of the Art

Table VII summarizes the parameters for the proposed $0.14\lambda_0$ and $0.11\lambda_0$ profile antennas and compared with reported works. Due to the very wide bandwidth of the proposed antennas, the lower edge frequency was chosen for the electrical length of the proposed dipoles and reported

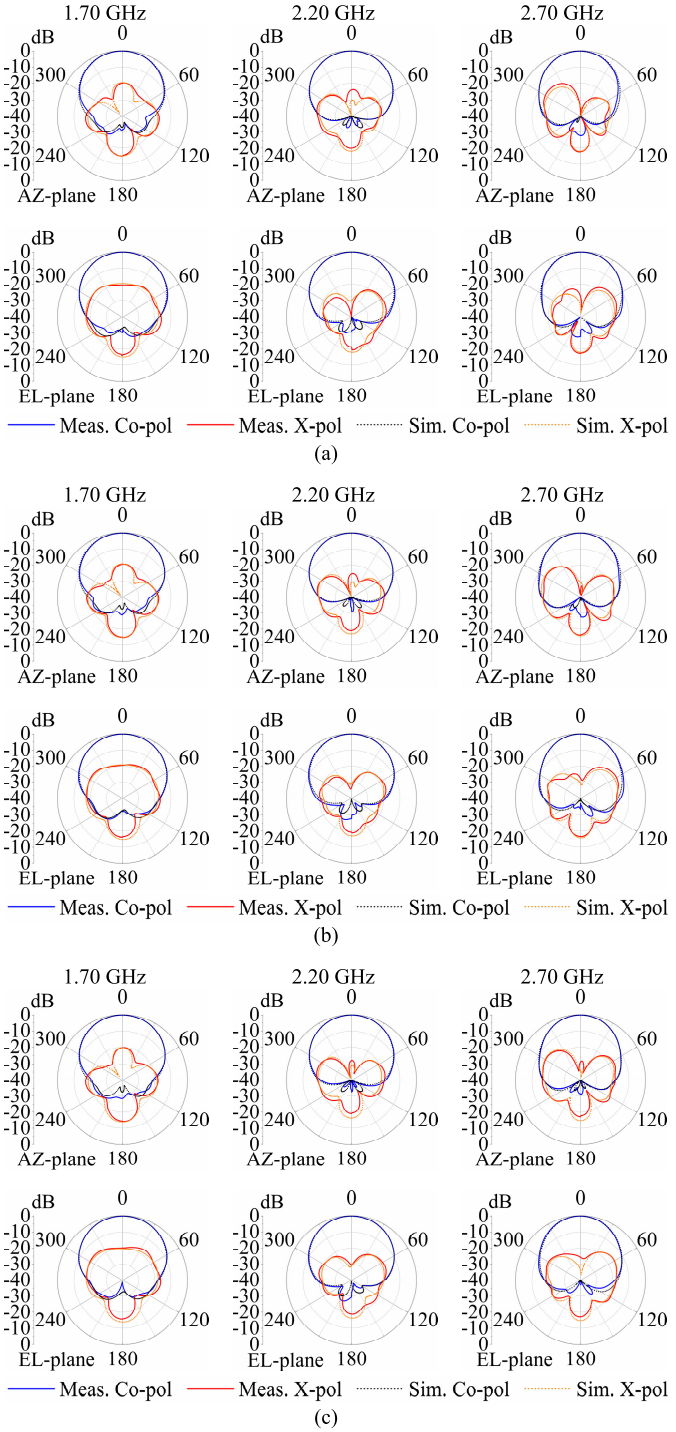

Fig. 12. Measured and simulated patterns for −45° polarized dipole with (a) 2 × 2 elements, (b) 3 × 3 elements, and (c) 4 × 4 elements in the *AZ*-plane and EL-plane at 1.7, 2.2, and 2.7 GHz.

works. First, the proposed dipoles are TM and TE surface wave antennas with four resonances generated by the metasurface layer. There are only two or three resonances found in [4], [5], [6], [7], [8], [9], [10], and [11]. Since half-wavelength dipoles or crossed dipoles are used to excite the metasurface layer in [4], [5], [6], [7], [8], [9], and [10], both the dipole and metasurface layer are contributing to the resonances. Besides that, the proposed metasurface dipole arms are fully integrated

with the metasurface layer on a single substrate. The dipole and metasurface layers are separated in [4], [5], [6], [7], [8], [8], [9], and [10]. Two substrates were used in [4], [5], [7], [9], and [10], whereas single substrate was used in [6] and [8] to widen the impedance bandwidth. Although the metasurface layer is fully integrated in [11], it is a metasurface microstrip patch antenna. Moreover, the proposed crossed-feed structure consisting of four chamfered patches ranging from $0.092\lambda_0$ to $0.155\lambda_0$ used to excite the metasurface layer is electrically smaller than the conventional excitation using a half-wavelength dipole or crossed dipoles [4], [5], [6], [7], [8], [9], [10]. However, a metasurface patch antenna is used in [11] with $0.16\lambda_0$ feed line. The proposed $0.14\lambda_0$ profile metasurface dipoles have 14-dB impedance bandwidths much wider than all metasurface antennas [4], [5], [6], [7], [8], [9], [10], [11] and the proposed $0.11\lambda_0$ profile metasurface dipoles have 10-dB impedance bandwidths much wider than metasurface antennas [4], [5], [6], [7], [8], [9], [10], [11]. The 3-dB beamwidth for all proposed dipoles is acceptable. The 3-dB beamwidth for [4], [5], [6], [7], [8], [9], [10], and [11] except [5] does not meet the beamwidth recommendation [3] because of the fluctuating beamwidth. Even though [5] has a stable 3-dB beamwidth, the bandwidth is smaller than the proposed metasurface dipoles. The F/B >25 dB for all proposed metasurface dipoles, however [4], [5], [6], [7], [10], [11] do not meet the recommendation [3]. Ntawangaheza et al. [8] has F/B >30 dB, but the 10-dB bandwidth is smaller than all proposed metasurface dipoles. The isolation is >30 dB for all proposed dipoles. Overall, the proposed dipoles have several notable advantages including an electrically small crossed-feed structure, four resonances to generate very wide 10- and 14-dB impedance bandwidth, stable 3-dB beamwidth with less fluctuation, good XPD level, good F/B level, higher gain, low profile, extra low profile, and good isolation level. Most importantly, it is the only reported dual-slant metasurface integrated dipole on a single substrate providing considerable cost savings.

VI. Conclusion

The dual-slant metasurface crossed-dipole antenna exhibits four TM and TE surface wave resonances, generated by the metasurface layer. The metasurface is fully integrated into the dipole on a single substrate. Moreover, an electrically small crossed-feed structure is used to excite the metasurface layer compared to the conventional excitation using a half-wavelength dipole or crossed dipole. The metasurface dipoles have low profile with wide 14- and 10-dB impedance bandwidths, high gain, good isolation, and stable radiation patterns. Most importantly, a stable 3-dB beamwidth and good F/B level over the wide bandwidth is achieved, hence, an ideal low-cost candidate for base stations especially in multiband scenarios covering 2G to 5G services. Furthermore, the size of the metasurface dipole arm can be varied, maintaining the same bandwidth depending on the cellular base station applications. For less stringent 10-dB impedance bandwidth applications, the extra low-profile antenna is an ideal solution for UE applications.

Acknowledgment

The authors would like to thank MJ McAssey, Neville Tobella, and Errol Singleton from Alpha Wireless Ltd for antenna measurements support.

References

[1] Z. N. Chen, Q. Lou, and W. Liu, "Metantennas: Opportunities and challenges in future microwave metasurface antenna research and applications," in *Proc. 16th Eur. Conf. Antennas Propag. (EuCAP)*, Madrid, Spain, Mar. 2022, pp. 1–5.

[2] Z. N. Chen and K. M. Luk, *Antennas for Base Stations in Wireless Communications*. New York, NY, USA: McGraw-Hill, 2009, p. 183.

[3] J. Obermaier and J. Rumold, *Recommendation on Standards for Passive Base Station Antennas*, vol. 12. Düsseldorf, Germany: NGMN Alliance, Jan. 2022, pp. 30–44. Accessed: Apr. 3, 2024. [Online]. Available: https://www.ngmn.org/publications/ngmn-basta-passive-antennas-wp.html

[4] S. S. Syed Nasser and Z. N. Chen, "Low-profile broadband dual-polarization double-layer metasurface antenna for 2G/3G/LTE cellular base stations," *IEEE Trans. Antennas Propag.*, vol. 70, no. 1, pp. 75–83, Jan. 2022.

[5] H. Zhu, Y. Qiu, and G. Wei, "A broadband dual-polarized antenna with low profile using nonuniform metasurface," *IEEE Antennas Wireless Propag. Lett.*, vol. 18, no. 6, pp. 1134–1138, Jun. 2019.

[6] G. Liu, X. Sun, X. Chen, D. Xiong, M. Li, and M.-C. Tang, "A broadband low-profile dual-linearly polarized dipole-driven metasurface antenna," *IEEE Antennas Wireless Propag. Lett.*, vol. 19, no. 10, pp. 1759–1763, Oct. 2020.

[7] B.-J. Chen and X.-S. Yang, "Compact dual-polarized filtering antenna based on differential feeding and double-layer metasurface," *IEEE Trans. Antennas Propag.*, vol. 71, no. 1, pp. 1065–1070, Jan. 2023.

[8] J. D. D. Ntawangaheza, L. Sun, Z. Xie, Y. Pang, Z. Zheng, and G. Rushingabigwi, "A single-layer low-profile broadband metasurface antenna array for sub-6 GHz 5G communication systems," *IEEE Trans. Antennas Propag.*, vol. 69, no. 4, pp. 2061–2071, Apr. 2021.

[9] F. Costa, O. Luukkonen, C. R. Simovski, A. Monorchio, S. A. Tretyakov, and P. M. de Maagt, "TE surface wave resonances on high-impedance surface based antennas: Analysis and modeling," *IEEE Trans. Antennas Propag.*, vol. 59, no. 10, pp. 3588–3596, Oct. 2011.

[10] S. S. Syed Nasser, W. Liu, and Z. N. Chen, "Wide bandwidth and enhanced gain of a low-profile dipole antenna achieved by integrated suspended metasurface," *IEEE Trans. Antennas Propag.*, vol. 66, no. 3, pp. 1540–1544, Mar. 2018.

[11] W. E. I. Liu, Z. N. Chen, and X. Qing, "Broadband low-profile L-probe fed metasurface antenna with TM leaky wave and TE surface wave resonances," *IEEE Trans. Antennas Propag.*, vol. 68, no. 3, pp. 1348–1355, Mar. 2020.

[12] G. Goubau, "Multi-element monopole antennas," in *Proc. Workshop Electrically Small Antennas (ECOM)*, Ft. Monmouth, NJ, USA, May 1976, pp. 63–67.

[13] F. Yang and Y. Rahmat-Samii, "A unified approach: Hybrid FDTD/ARMA method, frequency band gap for surface wave propagation," in *Electromagnetic Band Gap Structures in Antenna Engineering*. Cambridge, U.K.: Cambridge Univ. Press, 2009, pp. 45–47.

Kok Loon Wong (Member, IEEE) received the M.Sc. degree in telecommunications from Queen's University Belfast, Belfast, U.K., in 2010. He is currently pursuing the Ph.D. degree in electronic engineering with Technological University Dublin, Dublin, Ireland.

From 2011 to 2024, he served as an Antenna Engineer with Alpha Wireless Ltd., Portlaoise, Ireland. He is a Senior Research Assistant with the Antenna and High-Frequency Research Center, School of Electrical and Electronic Engineering, Technological University Dublin. His research interests include electromagnetic theory, base station antennas, frequency selective surface, metasurface antennas, and mmWave antenna technologies.

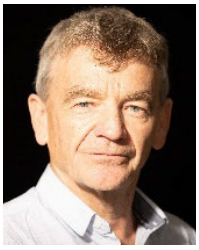

Max J. Ammann (Fellow, IEEE) received the Ph.D. degree in antennas and propagation from Trinity College, University of Dublin, Dublin, Ireland, in 1997.

He became a Chartered Engineer in 1986. He is a Professor of antennas and propagation with School of Electrical and Electronic Engineering, Technological University Dublin, Dublin, and the Director of the Antennas and High-Frequency Research Centre, Dublin. He has more than 200 peer-reviewed papers published in journals and international conferences. His research interests broadly include electromagnetic theory, antenna miniaturization for terminal and ultrawideband applications, antennas for medical devices, and mmWave antenna technologies.

Dr. Ammann is a member of the IEEE International Committee for Electromagnetic Safety. His team has received 14 Best Paper Awards at International Conferences on Antennas and Propagation and seven Commercialization Awards. He has served as an expert to industry on various antenna technologies in the communications, medical, aviation, and electronic security sectors in Ireland and Abroad. He acted as an Associate Editor for the IEEE ANTENNAS AND WIRELESS PROPAGATION LETTERS from 2012 to 2018. He has Co-Chaired IWAT2022 in Dublin and various workshops on antennas and related technologies.

Ming Cao received bachelor's degree in psychology from Peking University, Beijing, China, in 2005, and the master's degree in psychology from Sun Yat-sen University, Guangzhou, China, in 2007.

He completed the graduate training program in electronics and communication engineering from Tsinghua University, Beijing, in 2010. He is currently the RF Manager of Alpha Wireless Ltd., Portlaoise, Ireland. He joined Alpha Wireless in 2013. He began his career with Comba Telecom, Guangzhou, China, as an Antenna Design Engineer, in 2008. He is actively involved in development of a variety of antenna models, and he is well-versed of lifespan management for antenna products.

Fergal Lawlor (Member, IEEE) received the bachelor's and master's degrees in electronic engineering from the University of Limerick, Limerick, Ireland, in 1997 and 2005, respectively.

He is the Founder and CEO of Alpha Wireless Ltd., Portlaoise, Ireland. He has 30 years' experience in the telecommunications industry, having started his career as an RF Technician with Irish Defence Forces, before spending four years with Argus Technologies, Bella Vista, NSW Australia as an Antenna Designer. In 2001, he returned to Ireland and worked for sigma wireless and PCTEL as an Antenna Designer before starting alpha wireless. He has extensive experience in base station antenna designs and is recognized as a leading innovator in the CBRS/3.5-GHz space. He holds a number of antenna related patents.